



Digital Beam Steering Device Based on Decoupled Birefringent Prism Deflector and Polarization Rotator

Oleg Pishnyak, Lyubov Kreminska, and Oleg D. Lavrentovich
Liquid Crystal Institute, Kent State University, Kent, Ohio

John J. Pouch and Felix A. Miranda
Glenn Research Center, Cleveland, Ohio

Bruce K. Winker
Rockwell Scientific Company LLC, Thousand Oaks, California

The NASA STI Program Office . . . in Profile

Since its founding, NASA has been dedicated to the advancement of aeronautics and space science. The NASA Scientific and Technical Information (STI) Program Office plays a key part in helping NASA maintain this important role.

The NASA STI Program Office is operated by Langley Research Center, the Lead Center for NASA's scientific and technical information. The NASA STI Program Office provides access to the NASA STI Database, the largest collection of aeronautical and space science STI in the world. The Program Office is also NASA's institutional mechanism for disseminating the results of its research and development activities. These results are published by NASA in the NASA STI Report Series, which includes the following report types:

- **TECHNICAL PUBLICATION.** Reports of completed research or a major significant phase of research that present the results of NASA programs and include extensive data or theoretical analysis. Includes compilations of significant scientific and technical data and information deemed to be of continuing reference value. NASA's counterpart of peer-reviewed formal professional papers but has less stringent limitations on manuscript length and extent of graphic presentations.
- **TECHNICAL MEMORANDUM.** Scientific and technical findings that are preliminary or of specialized interest, e.g., quick release reports, working papers, and bibliographies that contain minimal annotation. Does not contain extensive analysis.
- **CONTRACTOR REPORT.** Scientific and technical findings by NASA-sponsored contractors and grantees.

- **CONFERENCE PUBLICATION.** Collected papers from scientific and technical conferences, symposia, seminars, or other meetings sponsored or cosponsored by NASA.
- **SPECIAL PUBLICATION.** Scientific, technical, or historical information from NASA programs, projects, and missions, often concerned with subjects having substantial public interest.
- **TECHNICAL TRANSLATION.** English-language translations of foreign scientific and technical material pertinent to NASA's mission.

Specialized services that complement the STI Program Office's diverse offerings include creating custom thesauri, building customized databases, organizing and publishing research results . . . even providing videos.

For more information about the NASA STI Program Office, see the following:

- Access the NASA STI Program Home Page at <http://www.sti.nasa.gov>
- E-mail your question via the Internet to help@sti.nasa.gov
- Fax your question to the NASA Access Help Desk at 301-621-0134
- Telephone the NASA Access Help Desk at 301-621-0390
- Write to:
NASA Access Help Desk
NASA Center for Aerospace Information
7121 Standard Drive
Hanover, MD 21076



Digital Beam Steering Device Based on Decoupled Birefringent Prism Deflector and Polarization Rotator

Oleg Pishnyak, Lyubov Kreminska, and Oleg D. Lavrentovich
Liquid Crystal Institute, Kent State University, Kent, Ohio

John J. Pouch and Felix A. Miranda
Glenn Research Center, Cleveland, Ohio

Bruce K. Winker
Rockwell Scientific Company LLC, Thousand Oaks, California

National Aeronautics and
Space Administration

Glenn Research Center

Acknowledgments

We thank Phil Bos for numerous useful discussions. The work was supported by NASA grant NAG3-2539 and by Rockwell Scientific Company LLC.

This report contains preliminary findings, subject to revision as analysis proceeds.

Available from

NASA Center for Aerospace Information
7121 Standard Drive
Hanover, MD 21076

National Technical Information Service
5285 Port Royal Road
Springfield, VA 22100

Available electronically at <http://gltrs.grc.nasa.gov>

Digital Beam Steering Device Based on Decoupled Birefringent Prism Deflector and Polarization Rotator

Oleg Pishnyak, Lyubov Kreminska, and Oleg D. Lavrentovich
Liquid Crystal Institute
Kent State University
Kent, Ohio 44242

John J. Pouch and Felix A. Miranda
National Aeronautics and Space Administration
Glenn Research Center
Cleveland, Ohio 44135

Bruce K. Winker
Rockwell Scientific Company LLC
Thousand Oaks, California 91360

Abstract

We describe digital beam deflectors (DBDs) based on liquid crystals. Each stage of the device comprises a polarization rotator and a birefringent prism deflector. The birefringent prism deflects the beam by an angle that depends on polarization of the incident beam. The prism can be made of the uniaxial smectic A (SmA) liquid crystal (LC) or a solid crystal such as yttrium orthovanadate (YVO₄). SmA prisms have high birefringence and can be constructed in a variety of shapes, including single prisms and prismatic blazed gratings of different angles and profiles. We address the challenges of uniform alignment of SmA, such as elimination of focal conic domains. Rotation of linear polarization is achieved by an electrically switched twisted nematic (TN) cell. A DBD composed of N rotator-deflector pairs steers the beam into 2^N directions. As an example, we describe a four-stage DBD deflecting normally incident laser beam within the range of ± 56 mrad with 8 mrad steps. Redirection of the beam is achieved by switching the TN cells.

1 Introduction

Beam steering devices are in a great demand in space communication, optical fiber communications, optical switches, scanners,¹⁻⁵ etc. In addition to classical devices such as gimbals and mirrors, a number of other techniques is being under development nowadays, such as ceramic-based phase gratings,² micro-electromechanical relief gratings,³ micromirror devices,⁴ decentered lens arrays, thermo-optic deflectors,⁵ photonic crystals⁶⁻⁸ etc. Non-mechanical compact devices that are free of inertia problems are certainly the most sought-after. Liquid crystals are of especial interest as active materials in non-mechanical beam steerers and deflectors, because of their structural flexibility, low operating voltage and low-cost fabrication.^{1,9} Recent advances in synthesis of new LC materials¹⁰ and in the design of the nematic LC cells¹¹ significantly improved parameters important for effective beam steering, such as optical birefringence and response times.

One of the most promising areas for LC-based systems is NASA's near-Earth and deep-space missions that require precise, diffraction-limited (sub-microradian), electronic (non-mechanical) beam steering as well as in situ wave-front correction. LC-based systems are inexpensive, light-weight and low-power. LC optical phased arrays could be used as part of a tracking network that supports high-data-rate communications links between the planetary rovers, the host lander, the orbiting spacecraft, and space platforms; autonomous operation of the rovers and robotic systems; and possibly strategic mining operations.

The most popular liquid crystal-based beam steering devices are based on diffractive and prismatic designs. Diffractive LC devices are known at least since 1970-ies, when Borel et al. described a binary rectangular LC diffraction grating.¹² This approach has been expanded by an optical-array beam steerers,^{1,13-22} polymer-dispersed liquid crystal gratings,^{23,24} ferroelectric liquid crystal gratings,^{25,26} photonic crystals filled with liquid crystals^{6,7} and voltage-controlled cholesteric liquid crystal gratings capable of both Raman-Nath and Bragg diffraction.²⁷⁻³⁰

Among the prism-based DBDs, one of the most effective designs uses a cascade of elementary stages each of which represents a pair of an active polarization rotator and a prismatic deflector.³¹⁻³⁸ The advantage of such a decoupled design is that it allows one to separate the issue of the short response time (determined mostly by the switching speed of the rotator) and the angular range of deflection (determined by the geometry and optical properties of the deflector). For example, the active element can be electrically switched by a twisted nematic (TN) cell followed by a passive birefringent prism that separates the beam into two channels, depending on the beam polarization (Fig.1). The decoupled pair of a rotator and deflector has no moving parts and can be cascaded into N stages, making 2^N addressable beam directions.

The liquid crystals can be used in both active and passive elements of prism-based DBD, as they demonstrate a relatively high optical birefringence (in the range 0.1-0.4) and relatively fast switching speed (milliseconds), see, for example, Ref. [11].

Application of LCs for polarization switching is a well-developed field, mostly because the TN and similar nematic cells are at the heart of modern LC display devices.³⁹

In this article we describe a four-stage DBD switched by four TN cells. The TN cells are coupled to the passive solid crystal (yttrium orthovanadate) prisms. The DBD switches optical beam at 633 nm in the range ± 56 mrad with 8 mrad steps. Application of LCs in the passive prismatic elements is less studied, despite their apparent advantages, such as structural flexibility and low-cost fabrication. One of the reasons for such a neglect is that a LC-based prism with a substantial dihedral angle α (needed for the substantial angle of beam deflection) and a substantial aperture A should be relatively thick, up to $h = A \tan \alpha$. If h is in the range of millimeters and centimeters, then huge losses caused by light scattering at director fluctuations^{40,41} rule out the applicability of the nematic LCs. In this article we describe passive prismatic element formed by a uniaxial SmA LC and by solid crystals. The advantage of the SmA materials over nematic LCs is that director fluctuations are suppressed by the layered smectic structure.

The article is organized as follows. Section 2 presents two types of birefringent materials for birefringent prisms, namely SmA LC materials and YVO₄ crystal and discusses the alignment procedures of SmA. Section 3 presents optical properties of single prisms and array of polymer prisms filled with SmA, birefringent YVO₄ Rochon biprisms and TN optical rotators. In Section 4, we characterize the assembled four-stage DBD based on TN cells and YVO₄ Rochon biprisms. Discussion and conclusions are presented in Sections 5 and 6, respectively.

2 Birefringent materials

The principal scheme of a rotator-deflector pair is shown in Fig.1. Depending on the applied voltage, the TN cell rotates the polarization of incident light by $\pi/2$ (no field, OFF state) or leaves the polarization intact (when the applied electric field reorients the liquid crystal molecules perpendicular to the plates of the cell, ON state). Inside the prism, the beam propagates as ordinary or extraordinary mode, depending on the polarization. As the ordinary and extraordinary refractive indices are different, the two modes of propagation through the prism result in different angle of deflection. As clear from Fig.1, if the SmA prism is used, the optical axis (and thus the preferred orientation of the SmA molecules) should be aligned along the edge of the wedge. In this geometry the director field is uniform everywhere.

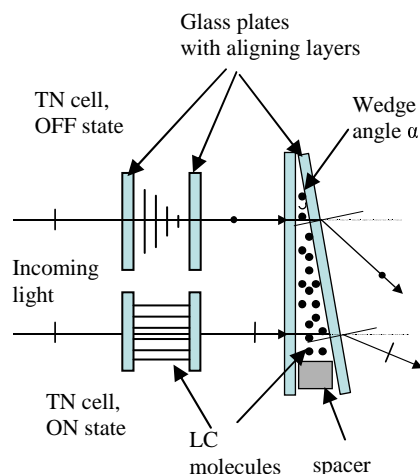


Fig.1. The principal scheme of a beam deflecting stage, composed of the switchable polarization rotator (TN cell) and a passive prism made of a SmA wedge. Both elements can be replaced: for example, a crystalline prism can be used as a deflector or an electrically-controlled birefringence cell can be used as a polarization rotator.

2.1 SmA LC materials

In SmA, the elongated rod-like molecules are arranged in a periodic stack of layers with the director \mathbf{n} (a unit vector that shows the average local direction of molecules and thus the optic axis of the material) being perpendicular to the layers; the states \mathbf{n} and $-\mathbf{n}$ are identical. Inside the layer the molecular centers of gravity show no long-range order, thus each layer is a two-dimensional fluid. Positional order along \mathbf{n} significantly reduces thermal director fluctuations and thus reduces light scattering^{40, 41}. However, the very same layered structure brings about another possible source of scattering, namely, static director distortions such as undulations and focal conic domains (FCDs).⁴²

Usually, the LCs are aligned by an appropriate treatment of the bounding plates of the cell (e.g., buffing of a thin polyimide layer). In flat nematic cells such an alignment is often sufficient to achieve a monodomain state. In SmA, however, even perfect surface alignment does not exclude undulations and FCDs as they can be caused by the mechanical response of the cell to varying temperature or by a small foreign particle in the bulk. To eliminate undulations and FCD in SmA, one might use a strong magnetic or electric field. However, as shown by Luckhurst et al., SmA samples are still hard to align as monodomains.^{43,44} Below we quantify the process of field alignment of SmA, by considering the behavior of a FCD in an applied magnetic field.⁴²

FCD can be stabilized by a mechanical impurity in the bulk or at the surface of the cell, or emerge as the result of the preceding undulation (periodic tilt and dilation) of SmA layers.⁴² These undulations can be caused by shrinkage of the SmA layers when the material is cooled down (cooling is needed as the cell filling is facilitated at high temperatures when the viscosity is low). As molecular layers in many SmA materials, such as cyanobiphenyls, are composed by pairs of oppositely oriented polar molecules, their thickness can vary significantly, from the value close to the length of one molecule to about twice of this value. These polar materials are especially hard to align.⁴⁵ Non-polar SmA show one-molecule layers with thickness that is not so strongly affected by temperature.

The known description of undulations^{39,40} refers to the case when the molecules are aligned perpendicularly to the bounding plates (homeotropic alignment). In our case, however, the plates set planar orientation with the molecules aligned parallel to the plates and to the dihedral edge of the prism, Fig.1. Nevertheless, we observed that even in this case, cooling of the SmA material such as 4-octyloxy-4'-cyanobiphenyl (8OCB) results in layers undulations and subsequent formation of parabolic FCDs, Fig.2. The physical mechanism of this process remain to be explained, as the geometry of confinement is different from that in classical undulation scheme, but one can still obtain a close estimate of the magnetic field needed to align the SmA uniformly, by considering the behavior of the FCDs, as the FCDs are the most developed departures from the uniform alignment of SmA. We consider the simplest type of FCD, the so-called toric FCD that can be stabilized by a foreign particle in the SmA bulk,^{46,47} Fig.3.

The toric FCD is based on a pair of linear defects, a circular defect line and the straight line passing through the center. The smectic layers are wrapped around the pair as shown in Fig.3. Note that outside the FCD the molecules are oriented uniformly along a single axis parallel to the plates.

Suppose a small toric FCD with the radius a of the defect circle much smaller than the lateral size of the cell, is stabilized in an otherwise uniform SmA sample by a particle, which sets tangential orientation of SmA molecules at its surface. For the sake of simplicity, we approximate the particle by a disk of radius R and zero thickness, Fig.3. If the SmA were uniform, the director would be in an unfavorable perpendicular orientation at the plate. The FCD would be stable if its elastic energy⁴⁸

$$F_{el} = 2\pi^2 a K \left[\ln(2a/r_c) - 2 - \bar{K}/K \right] + F_c, \quad (1)$$

(where K is the splay elastic constant, \bar{K} is the saddle-splay constant, r_c is the core radius of the circular defect, and F_c is the core energy of the circle and the straight line) is smaller than the anchoring energy difference between the FCD-free (uniform) state and the FCD state:

$$\Delta F_s = 2\pi a^2 W, \quad (2)$$

where W is the surface anchoring coefficient for director deviations in the plane normal to the particle's surface, the so-called polar anchoring coefficient. In SmA, $W \sim (10^{-3} - 10^{-2}) \text{ J/m}^2$ is orders of magnitude higher than the corresponding value in the nematic phase, where typically $W \sim (10^{-5} - 10^{-4}) \text{ J/m}^2$.⁴⁹

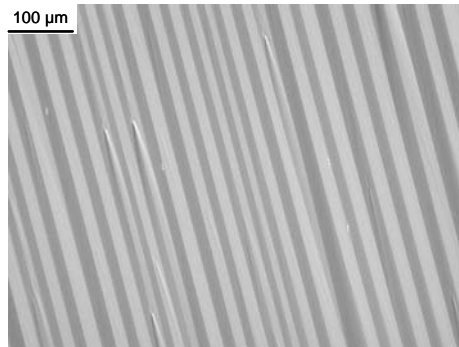


Fig.2. Polarizing-microscope texture of an undulation pattern in SmA material 8OCB created by periodic director variations. The SmA was cooled down from the magnetically aligned nematic phase. Aligning layer: polyisoprene, no rubbing.⁵⁰ Cell thickness 5 μm.

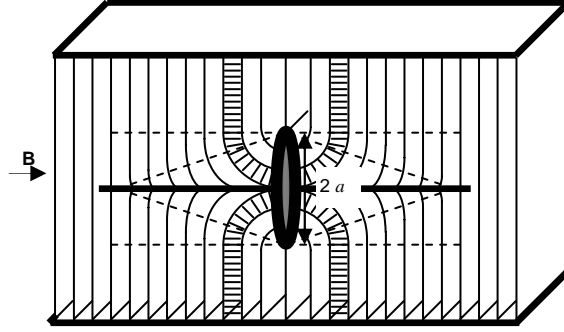


Fig.3. Schematic view of toric FCD. The SmA layers are perpendicular to the substrates and folding within the FCD. The director changes the orientation on 90° from tangential outside the FCD to vertical within the FCD to satisfy the boundary conditions at the disk-like foreign particle in the SmA bulk.

If the anisotropy $\chi_a = \chi_{\parallel} - \chi_{\perp} > 0$ of SmA diamagnetic susceptibility is positive, then applying the field in the direction of the desired orientation of molecules should reduce the FCD, as the molecules inside the domain should reorient along \mathbf{B} , Fig.3. The diamagnetic energy gain from such a reorientation is $\Delta F_B = \int \frac{1}{2} \mu_0^{-1} \chi_a B^2 \sin^2 \theta dV$, where $\mu_0 = 4\pi \times 10^{-7} \text{ N/A}^2$ is the permeability of free space, θ is the angle between the director and \mathbf{B} , the volume element is $dV = r(a - r/\sin \theta) \sin \theta d\theta d\varphi dr$; r and $r - a/\sin \theta$ are the principal radii of curvature of SmA layers within the toric FCD, r varies in the range from 0 to $a/\sin \theta$; $0 \leq \theta \leq \pi/2$; $0 \leq \varphi < 2\pi$. Integration yields

$$\Delta F_B = \frac{1}{6} \mu_0^{-1} \chi_a B^2 a^3, \quad (3)$$

The stability of the FCD is determined by the energy difference between the FCD state and the uniform state, comprised of the elastic, surface anchoring, and diamagnetic contributions, $\Delta F = \Delta F_s - F_{el} - \Delta F_B$:

$$\Delta F = 2\pi a^2 W - 2\pi^2 a K \left[\ln \frac{2a}{r_c} - 2 - \frac{\bar{K}}{K} \right] - F_c - \frac{1}{6} \mu_0^{-1} \chi_a B^2 a^3 \quad (4)$$

Figure 4 shows the function $\Delta F(B)$ for two different sizes of FCDs, of radius $a = 1 \mu\text{m}$ and $0.4 \mu\text{m}$, calculated for the following typical values of parameters:

$K = 10^{-11} \text{ N}$, $\bar{K} = 0$, $W = 10^{-2} \text{ J/m}^2$, $r_c = 10 \text{ nm}$, $F_c = 0$ (r_c is chosen to adsorb the core energy into the elastic energy of layers distortions⁴²), and $\chi_a = 10^{-5}$.⁴⁹ The plot clearly demonstrates that to reduce the size of FCD to sub-wavelength (in visible and near-IR) scale, one would need huge magnetic fields of the order of tens and hundreds of Tesla.

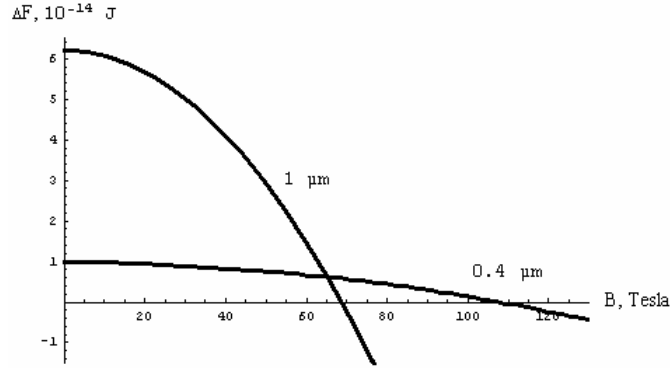


Fig.4. Free energy difference between the uniform state of a SmA slab with an incorporated foreign particle-disk and the state with the toric FCD, as the function of the magnetic field applied to align the director uniformly.

Now let us compare this estimate to the magnetic field needed to realign the director around a foreign particle in the nematic phase, where the polar anchoring is usually much weaker. The magnetic field would be able to realign the director around a foreign particle

completely when the corresponding diamagnetic coherence length $\xi = \frac{1}{B} \sqrt{\frac{\mu_0 K}{\chi_a}}$ is

smaller than the anchoring extrapolation length $l = \frac{K}{W}$, i.e. when the magnetic field is larger than

$$B_c = W \sqrt{\frac{\mu_0}{K \chi_a}}. \quad (5)$$

Therefore, $B \sim 1 \text{ T}$ would be sufficient to suppress the director distortions around a particle with $W \sim 10^{-5} \text{ J/m}^2$; $B \sim 10 \text{ T}$ would be needed if $W \sim 10^{-4} \text{ J/m}^2$, etc. Therefore, magnetic alignment is much easier in the nematic phase than in the SmA phase.

Consideration above suggests that in order to minimize the light losses, one should search for the SmA material composed of nonpolar molecules, which has not only a SmA but also a nematic phase. The material can be aligned in the nematic phase and then slowly cooled down to the SmA phase to obtain a low-scattering birefringent sample.

The requirements above are met by low-molecular weight 4,4'-*n*-dialkylazoxybenzenes as demonstrated first in Ref. [31,32], Fig.5a. We developed these materials further and used *n*=5,6,7,8 homologues of 4,4'-*n*-dialkylazoxybenzene purchased from Sigma-Aldrich Chem. Co to prepare mixtures with a broad temperature range of SmA phase. All the LC components were purified to decrease the contents of

undesired dopants and foreign particles. The purification process was as follows: first we dissolved the compound in methanol (99.93%, Aldrich) in proportion 1 gram of LC in 100 ml of methanol. Then the solution was cooled down to separate the crystal from the methanol. The precipitated crystals were filtered and dried out. The purified compounds were mixed in various proportions to get the appropriate phase sequence and a good alignment. The temperature range of SmA phase can be expanded to about 30 degrees in eutectic mixtures. The mixture of $n=6$ and $n=8$ homologues in proportion 1:1 shows the best deflection efficiency (a ratio of intensities of the deflected and incident beams) and a good thermal range, Fig.5b. These mixtures were used as a SmA filler for passive prismatic deflectors.

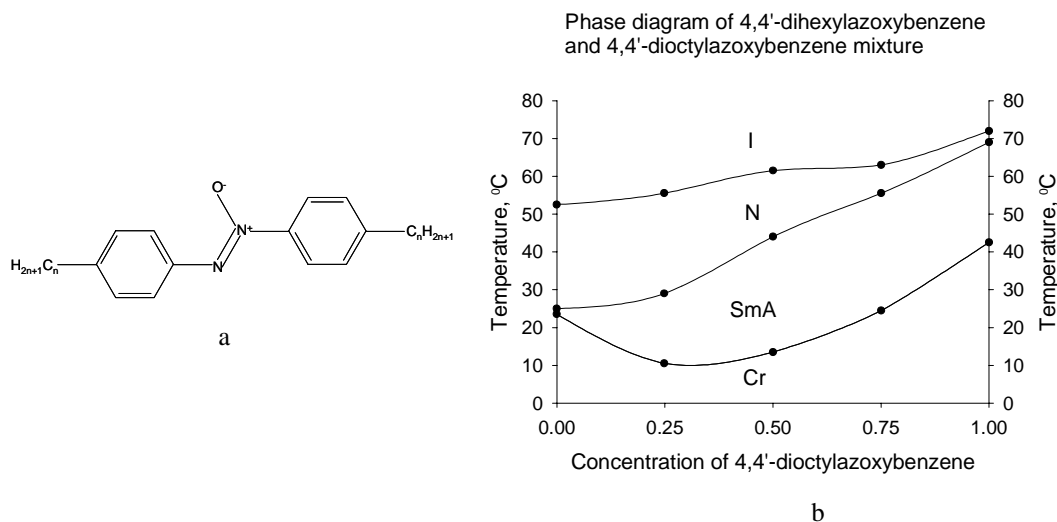


Fig.5. Molecular structure of 4,4'- n -dialkylazoxybenzene (a); Phase diagram of the binary mixture of $n=6$ and $n=8$ homologues of 4,4'- n -dialkylazoxybenzene (b).

2.2 Yttrium orthovanadate crystal

SmA liquid crystals might serve as good materials to construct inexpensive, large-aperture birefringent elements such as prismatic deflectors. The advantages of SmA are especially evident when complex geometries are needed, e.g., prisms with curved surfaces. However, SmA are still hard to align and when high-quality optical performance is needed, regular solid crystal prisms might be preferable.

We have chosen solid crystal yttrium orthovanadate YVO_4 as the high-optical quality material for the passive beam deflectors. YVO_4 is an optically positive uniaxial crystal of a tetragonal structure with a large birefringence ($n_o = 1.9929$, $n_e = 2.2154$, and $\Delta n = n_e - n_o = 0.2225$ at $\lambda = 633$ nm), a wide transparency range (400-5000 nm) and good temperature stability. Modern technology¹ allows for the growth of large aperture homogeneous crystals (few centimeters) enabling fine optical polishing of the working surface.

Large birefringence of YVO_4 crystal is an advantage when one needs to obtain a large deflection angle. However, high indices n_o and n_e of the crystal cause large Fresnel

¹ <http://www.crystalsland.com/yvo.html>

reflection, thus decreasing the efficiency of the device and producing bounced beams in optical system. We estimated the reflection by single YVO₄/air interface to be 11% for the ordinary wave and 14% for the extraordinary wave (normal incidence, $\lambda=633$ nm) using Fresnel formulae.⁵¹ The total transmission through a system with eight YVO₄/air interfaces is only 39% of the incident ordinary wave and 30% of the extraordinary wave. An obvious remedy is to coat the YVO₄ with the antireflective coatings.

3 Optical elements: prisms, lattices and polarization rotators

In this section we describe properties and performance of optical elements used in single-stage beam-deflection schemes, namely, the SmA and solid YVO₄ prisms, SmA/acrylic prisms and rotators of polarization based on TN cells.

3.1 Single SmA prisms

The geometry of the prismatic cell filled with LC material is shown in Fig.1. Two glass plates with rubbed polyimide layers (PI2555, Microsystems) formed a wedge cell, which was filled with the SmA blend of 4,4'-dihexylazoxybenzene and 4,4'-dioctylazoxybenzene in proportion 1:1. The assembled cell was heated to the isotropic state and slowly cooled down to the room temperature with the temperature rate $\sim 5 \times 10^{-4}$ K/s in 1.2 Tesla magnetic field. The measured parameters of the birefringent prism are as following:

- wedge angle: 15.8° ;
- refractive indices of the SmA mixture (at $\lambda=633$ nm and temperature 22°C): $n_e = 1.72$, $n_o = 1.53$, $\Delta n = 0.19$;
- steering angles: for the light polarized parallel to the LC director (extraordinary wave) $\theta=12.2^\circ$, for the light polarized perpendicular to the LC director (ordinary wave) $\theta=8.9^\circ$.

The textures of the aligned mixture (Fig.6a) show small amount of residual FCDs. As the SmA mixture has a positive birefringence $\Delta n = n_e - n_o > 0$, the extraordinary wave will deflect more than the ordinary wave, Figs.6b-d. Both deflected beams show high efficiency at wavelength $\lambda=633$ nm, Fig.7. The data in Fig.7 are normalized to the incident light intensity I_0 . The decrease of transmission observed for some particular thickness of the wedge cell is caused by the light scattering on FCDs remained in some portions of the cell after the aligning procedure.

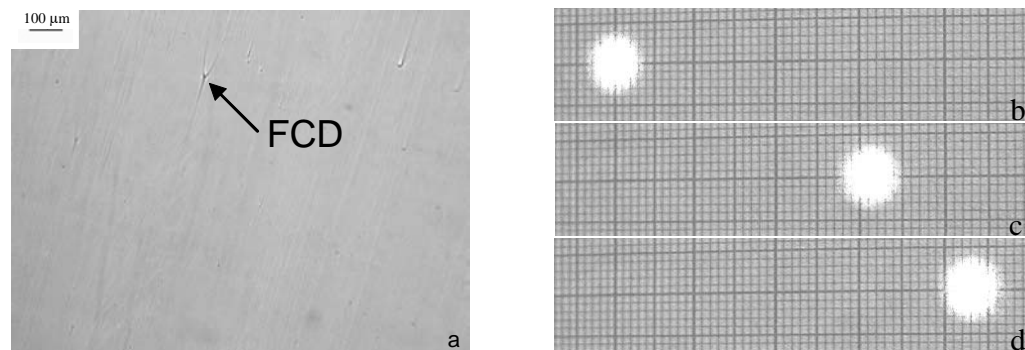


Fig.6. (a) Textures observations of the wedge cell filled with the SmA mixture after alignment in 1.2 Tesla magnetic field. Thickness of the cell $\sim 200 \mu\text{m}$, wedge angle $\sim 15.8^\circ$. (b) Position of the incident beam on the screen. (c) Position of the deflected ordinary beam passed through the wedge cell. (d) Position of the deflected extraordinary beam.

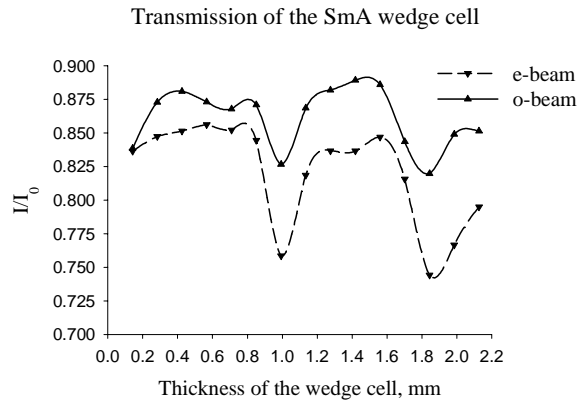


Fig.7. Transmission of the birefringent wedge cell at $\lambda = 633$ nm.

3.2 Polymer prisms array filled with SmA material

The assembling of the SmA-filled wedges for the wide-aperture incident beam is complicated and requires a lot of LC material. In this case a single birefringent prism may be substituted by an array of small prisms. Hirabayashi et al. reported on quartz microprisms filled with nematic material, which can deflect closely spaced micro-optical beams individually to any position with a high transmittance, high deflection angle and low voltage.⁵² Here we describe a passive birefringent element, namely an array of prisms filled with a SmA material. Right angle prisms may be molded in a sheet of polymer material with a different cut angle α and period d , Fig.8. We used the array of prisms with $\alpha=30^\circ$ and $d=1$ mm from Fresnel Technologies, Inc. Material of the prisms plate is optically quality acrylic with the refractive index $n=1.49$ (at $\lambda=589$ nm). The polymer plate was attached to a glass substrate coated with rubbed polyimide PI2555 (there is no aligning layer at the prisms surface). Then the assembled cell was filled with the mixture of 4,4'-dihexylazoxybenzene and 4,4'-dioctylazoxybenzene in proportion 1:1. After aligning in the magnetic field we measured the deflection efficiency and deflection angles of the cell at 633 nm wavelength and normal incidence (we considered zero-order diffracted beam, diameter of the incident beam was equal to 5 mm):

- for the extraordinary wave the deflection efficiency was $\sim 75.4\%$ and the deflection angle $\theta=7.1^\circ$;
- for the ordinary wave the deflection efficiency was $\sim 80.5\%$ and the deflection angle $\theta=0.7^\circ$.

The performance of the assembled cell is very similar to Rochon prisms, but due to slight mismatch between the acrylic refractive index and ordinary refractive index of the

LC material the ordinary wave is slightly deflected. The intensity losses are caused by: 1) light diffraction, as polymer array is a periodic structure; 2) destructive interference of different parts of the light beam acquiring different optical paths while passing through the cell; 3) light scattering caused by variations of the LC director (fluctuating and static) and by mechanical imperfections of the acrylic plate.

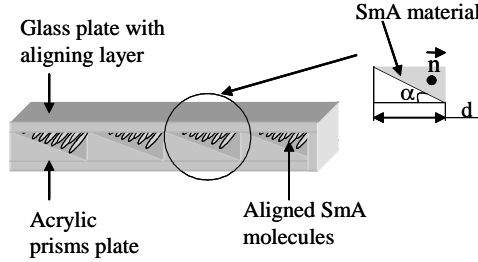


Fig.8. Array of polymer prisms filled with the SmA material.

3.3 Crystalline birefringent biprisms

We used Rochon biprisms⁵¹ made of the solid crystalline YVO_4 as passive birefringent discriminators in the assembled DBD. RP is composed of two prisms at wedge angle α and cemented together. The optical axes of two prisms are perpendicular to each other, Fig.9.

A beam with the E-vector oscillating in the plane of Fig.9 (p-wave, marked by bars) represents the ordinary wave for both prisms with the index of refraction n_o . This wave is transmitted without deflection. A beam with the E-vector oscillating perpendicularly to the plane of the figure (s-wave, marked by dots) is the ordinary wave in the first prism only, becoming an extraordinary wave in the second prism with the refractive index n_e . The deflection angle Θ^{out} (see Fig.9) of the normally incident wave depends on the optical birefringence Δn and wedge angle α of the RP, $\Theta_s^{out} = \Delta n \alpha$, or, if there is a small incident angle Θ_s^{in} ,

$$\Theta_s^{out} = \Delta n \alpha + \Theta_s^{in} \quad (6)$$

The wedge angle α of the RP that would change the angular direction of propagation from an incident angle Θ_s^{in} into a needed angle Θ_s^{out} is calculated as

$$\alpha = (\Theta_s^{out} - \Theta_s^{in}) / \Delta n. \quad (7)$$

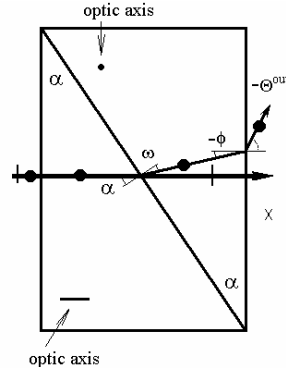


Fig.9. Scheme of the light propagation by the Rochon prism made from optically positive crystal for s-wave (marked by dot) and p-wave (marked by line). Angles are measured from the x-axis to the wave vector direction (taken as a positive when clockwise and as a negative when counterclockwise).

3.4 Polarization rotators

The 90° TN cells represent a good candidate for electrically-controlled polarization switchers because technology of their fabrication is well established; some drawbacks of these devices is their relative slow response (in the range of milliseconds). The cell is assembled from two glass plates with tangential director alignment along two mutually perpendicular axes at the opposite plates and filled with a slightly chiral nematic LC.

Depending on the applied voltage, the TN cell can be either in the state “OFF” or “ON”. In the OFF state, the cell rotates the polarization of linearly polarized beam by 90° . The emerging light remains linearly polarized only if the TN cell satisfies one of the two criteria: (1) either it is infinitely thick and satisfies the Mauguin limit ($\lambda \ll \Delta n d$) or (2) it is of the finite thickness d such that

$$d = \frac{\lambda}{2\Delta n} \sqrt{4m^2 - 1}; \quad m = 1, 2, 3, \dots \quad (8)$$

called the Gooch-Tarry or Mauguin minima.^{39,53} For the sake of simplicity we will refer to the wave with rotated polarization as the “ $\pi/2$ -wave” and will also call the OFF state of the TN cell as the “ $\pi/2$ -state”.

In the state “ON” of the TN cell, the direction of light polarization remains the same. A sufficiently strong applied voltage realigns the nematic director perpendicular to the plates and the optical activity disappears. For the sake of simplicity we denote this wave as “0-wave” and the ON state of the TN cell as “0 state”.

The 90° TN cells were assembled from two parallel glass plates treated for planar alignment and filled with the dual frequency nematic MLC-2048 material (purchased from EM Industries). MLC-2048 has a large birefringence $\Delta n = 0.221$ and can be switched extremely quickly, within tenths of a millisecond in relatively thick 10- μm cells.⁵⁴ The applied voltage reorients the director perpendicularly to the plates if its frequency is higher than 15 kHz (at room temperature); at lower frequencies, the voltage keeps the director parallel to the plates. A small amount of right hand chiral dopant⁵⁵ (molecular structure is shown in Fig.10, a) to MLC-2048 produced a right-handed twist

of the director. Glass spacers assured a thickness corresponding to the first Gooch-Tarry minimum condition at $\lambda = 633$ nm.

We tested the performance of the TN cells by placing them between a pair of polarizers, either crossed (for $\pi/2$ -wave test) or parallel (for 0-wave test). The typical transmission-voltage curves for normal light incidence are shown in Fig.10, b,c. We achieved the transmission coefficient 94% for the $\pi/2$ -wave and 97% for the 0-wave, by using TN cells with antireflection coatings. The coefficient is determined as the ratio of the output beam intensity to the incident beam intensity. The leakage of light of undesirable orthogonal polarization was less than 0.5 %.

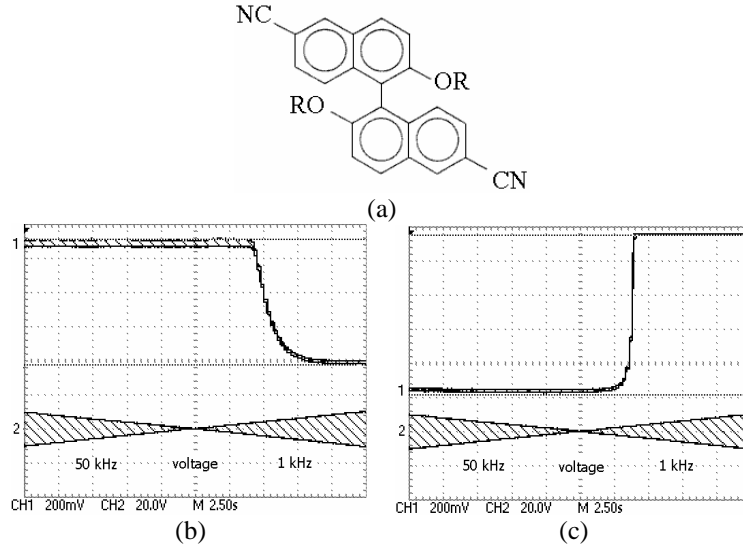


Fig.10. (a) Molecular structure of binaphthalene compound, $R=(CH_2)_9CH_3$. (b,c) Oscillograms of the TN cells transmission (curve 1b: crossed polarizer and analyzer and curve 1c: parallel polarizer and analyzer) vs applied voltage (curve 2) that decreased from 10 to 0 V at 50 kHz and then increased from 0 to 10 V at 1 kHz.

4 Design of the DBD

Modeling

We designed a DBD composed of four stages that deflects an incident He-Ne laser beam into $2^4 = 16$ directions within the range ± 56 mrad with 8 mrad steps, Fig.11. Each stage is composed of a TN cell as the polarization rotator and a solid crystal YVO_4 Rochon prism as the passive deflector. The maximum deflection angle increases by a factor of 2 from the first stage to the third stage. The fourth prism deflects into the opposite angular direction, as it is flipped with respect to all other prisms, as shown in Fig.11.

Table 1 shows the calculated wedge angles α of YVO_4 prisms that provide the required angular deviations $\Theta^{in} \rightarrow \Theta^{out}$ at $\lambda = 633$ nm, see Eq.(7). The four prisms with wedge angles specified in Table 1 were custom made by Conex Systems, Inc. and coated with the antireflective film by Thin Film Technology, Inc.

To illustrate the sequence of deflections, let us trace the contour beams of +8 mrad (s-wave) and -8 mrad (p-wave) transmitted through the proposed DBD. Let TNs at the stages 1, 2, and 3 do not change the polarization, while the fourth TN rotates the polarization state by 90° .

- (1) The first prism (RP1) increases the deflection angle of s-wave from +8 mrad to +16 mrad. The second prism (RP2) deflects the wave to +32 mrad. The third prism RP3 enlarges the angle to +64 mrad. The fourth TN changes the state of s-polarization into p-polarization. The p-wave passes the 4th prism (RP4) unaltered at +64 mrad.
- (2) The p-wave passes through the first three prisms without changing the input angle of -8 mrad. The fourth TN changes the state of p-polarization into s-polarization. The 4th prism (RP4) deviates this s-wave to -64 mrad.

As just demonstrated, the DBD expands the incident light sector of (-8; +8) mrad into the sector of (-64; +64) mrad. For the normally incident laser beam, the deflected directions are in the range (-56 mrad, +56 mrad). A small non-zero incident angle Θ^{in} change the range of deflection angles approximately as $(-56 \text{ mrad} + \Theta^{in}, +56 \text{ mrad} + \Theta^{in})$.

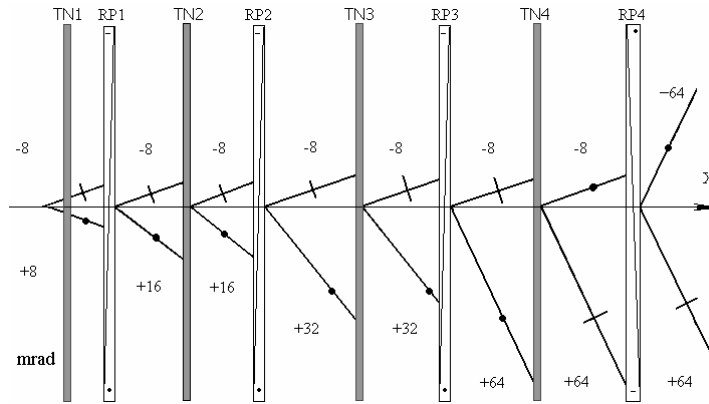


Fig.11. Sketch of the DBD device. Black bars and dots mark the direction of the optic axis of the RP. Angles are measured in mrad. For the sake of simplicity, wave normals start from the center of each optic element.

Table 1. RPs: the wedge angle α and deflection of an incident s-wave $\Theta^{in} \rightarrow \Theta^{out}$ polarized perpendicularly to the plane of Fig.9.

	RP1	RP2	RP3	RP4
$\Theta^{in} \rightarrow \Theta^{out}$, mrad	8 \rightarrow 16	16 \rightarrow 32	32 \rightarrow 64	8 \rightarrow 64
α , deg	2.06°	4.12°	8.20°	14.17°

Experimental setup

We assembled the DBD from four pairs of RP and TN as shown in Fig.11. All optical elements were placed on adjustable Newport Gimbal Optical Mounts. The He-Ne laser with the polarization ratio 200:1 was used as the source of linearly polarized coherent light at $\lambda = 633 \text{ nm}$.

The multi-channel Waveform Generator WFG 500 (FLC Electronics) was automated by computer to address the TN cells. We measured the light intensity by the Newport Optical Power Meter Model 835.

The pattern of steered beams was captured by the CCD-camera in the focal plane of the long-focusing convergent lens with the focal length $f=1$ m. We measured the output deviation angle in the focal plane of the lens as $\text{ArcTan}(\Delta/f)$, where Δ is the beam displacement. Each displacement by 1 mm corresponds to 1 mrad angle.

5 Experimental Results and Discussion

The DBD deviated the normally incident laser light into the range (-56 mrad, +56 mrad) with the step of 8 mrad as shown in Table 2. The addressing of TN cells was performed accordingly to the algorithm of Table 2. All deflection states are independent of each other.

Table 2 shows how four TNs control the deflection of a p-wave, as an example. The symbols “0” and “ $\pi/2$ ” means “polarization unchanged” and “polarization rotated by $\pi/2$ ”. The number NN marks the mode of operation of the whole set of TNs. For example, for the line NN=9 in Table 2, which corresponds to the “0000” mode, all four TN cells transmit the input light without deviation, the total deflection angle is 0 mrad. Switching of 4th TN to the rotation mode, “000 $\pi/2$ ”, results in the deflection angle $\Theta^{out} = -56$ mrad (line NN=1) and so on. There are sixteen deflected directions (direction “0 mrad” appears twice for p- and s-waves, NN 8,9). A slight mutual displacement of patterns NN8 and NN9 is caused by the finite manufacturing tolerance (1 mrad) of the fourth RP.

The light transmission of the DBD is strongly reduced by reflection losses at the crystal/air and glass/air interfaces because refractive indices of the used materials are different: $n_{\text{glass}} = 1.5$ for the glass, $n_o = 1.4978$, $n_e = 1.7192$ for the liquid crystal MLC-2048, and $n_o = 1.9929$, $n_e = 2.2154$ for YVO₄. The transmission can be increased in a number of ways, the most evident being the following two: by filling space between the optical elements with appropriate immersion fluids or by coating all relevant surfaces with antireflective films.

Figure 12 shows numerically simulated results for the DBD in which the space between all the elements is filled with the same immersion fluid. The transmission reaches a maximum of about 88% for both polarizations when the refractive index is $n_{rl}=1.8$.

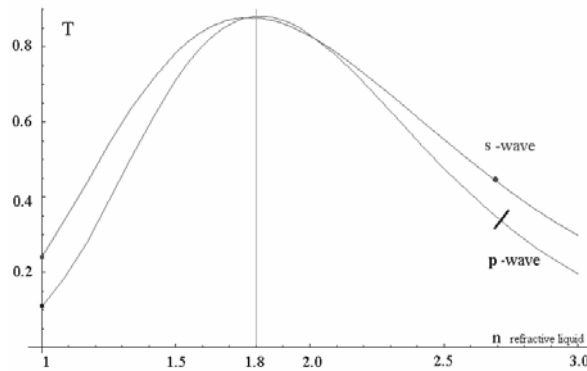















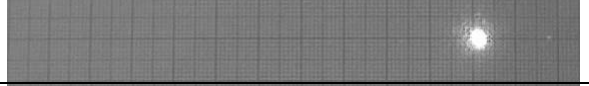


Fig.12. Light transmission of a DBD as the function of the refractive index of the immersion liquid for s- and p- waves.

To test the second approach, we constructed and tested the performance of DBD in which the surfaces of RPs and TN cells in contact with air were coated with antireflective films designed for $\lambda = 633$ nm. The resulting light transmission through the four-stage DBD increased to 75%. The intensity of the brightest parasitic beam caused by reflection at the interfaces was less than 1.6% of the intensity of incident light.

Note that reflection losses pose a problem not only for solid crystal prisms, but also for SmA-filled birefringent elements. Most of reflections occur at the air/substrate interfaces. If the substrate is made of glass, the reflection is about 4% at each interface.

Table 2. Sequence of patterns of laser beams steered by the DBD. Beams are displaced on 8 mm, that corresponds to the 8 mrad angle. All elements of the DBD had antireflection coating.

NN	Θ , mrad	Pattern	TN cells operation mode			
			TN1	TN2	TN3	TN4
1	-56		0	0	0	$\pi/2$
2	-48		$\pi/2$	$\pi/2$	0	$\pi/2$
3	-40		0	$\pi/2$	$\pi/2$	$\pi/2$
4	-32		$\pi/2$	0	$\pi/2$	$\pi/2$
5	-24		0	0	$\pi/2$	0
6	-16		$\pi/2$	$\pi/2$	$\pi/2$	0
7	-8		0	$\pi/2$	0	0
8	0		$\pi/2$	0	0	0
9	0		0	0	0	0
10	8		$\pi/2$	$\pi/2$	0	0
11	16		0	$\pi/2$	$\pi/2$	0
12	24		$\pi/2$	0	$\pi/2$	0

13	32		0	0	$\pi/2$	$\pi/2$
14	40		$\pi/2$	$\pi/2$	$\pi/2$	$\pi/2$
15	48		0	$\pi/2$	0	$\pi/2$
16	56		$\pi/2$	0	0	$\pi/2$

Let us underline the advantages that SmA-filled elements might have in comparison with YVO₄ prisms. First of all, SmA prisms are easier to prepare, as they do not require polishing and fine controlling of the optical axis during manufacturing, which is very critical in the case of crystalline prisms. The optical axis of SmA prisms can be easily set by the rubbing direction of the aligning polyimide or/and direction of the applied external field. SmA materials allow one to construct low-cost wide-aperture birefringent elements, while the aperture of YVO₄ prisms is limited by a few centimeters.

The transmission of a single SmA-filled prism is much better than a polymer array of prisms. However, the advantage of a grating is in the thickness of the device and thus in the quantity of the material used. One can reliably produce single SmA prisms with the aperture of about 20 mm and wedge angle of 20°, but larger dihedron angles and wider apertures are better to achieve with the prismatic arrays. The SmA prismatic arrays can work well for closely spaced small aperture optical beams (the aperture is smaller than the period of the polymer array), for example, in communication networks.⁵² In this case each microprism of the array serves as a single birefringent prism for the incident beam and we avoid the diffraction losses, which occur for large aperture incident beam. The way to reduce the diffraction losses of large beams is an optimization of the period and cut angle of the array.

Among the disadvantages of SmA-filled elements is light scattering at the residual FCDs, which remain after aligning process. The alignment of SmA material is sensitive to the abrupt temperature fluctuations as well. The SmA prisms can only operate within the temperature range of the SmA phase; drastic temperature changes might cause a complete misalignment of the material.

6 Conclusion

We demonstrated the principle of non-mechanical digital beam deflection based on decoupled pairs of electrically-controlled liquid crystalline polarization switchers such as TN cells and passive deflectors, such as SmA or crystalline birefringent prisms. The scheme allows one to separate the issue of time response and beam deflection angles and optimize these two parameters separately. For example, one can replace the TN cells with electrically-controlled birefringent cells based on dual-frequency nematic liquid crystals and achieve sub-millisecond response times.⁵⁴

The deflection angles can be optimized by the design of the birefringent prisms. Smectic A-filled prisms are attractive in low-cost applications where one needs large apertures,

large angles of deflection, and/or non-trivial geometries. We demonstrated that mixtures of homologues of 4,4'-*n*-dialkylazoxybenzene produce SmA phases with a broad temperature range of SmA existence (up to 30 degrees C for binary mixtures) with a relatively small number of residual defects such as focal conic domains. We demonstrated that typical magnetic fields needed to align the director field uniformly in the SmA phase is one-two orders of magnitude higher than the corresponding field needed to align the nematic phase. Therefore, SmA mixtures with a neighboring nematic phase are especially attractive for applications as birefringent fillers, as the system can be field-aligned in the nematic phase. We also described regular solid crystal birefringent prisms made of YVO₄.

We demonstrated that the decoupled rotator-deflector design allows one to assemble multiple beam-deflecting stages into one device with a broad range of deflected directions. As an example, we constructed and tested a four-stage DBD with 16 deflection directions in the angular range of +56 to -56 mrad (for normal incidence). We achieved high efficiency of the deflected beams up to 75%.

References

1. P. F. McManamon, E. A. Watson, T. A. Dorschner, L. J. Barnes, "Applications Look at the Use of Liquid-Crystal Writable Gratings for Steering Passive Radiation", *Opt. Eng.* 32(11), 2657-2664 (1993).
2. James A. Thomas and Yeshaiah Fainman, "Optimal Cascade Operation of Optical Phased-Array Beam Deflectors", *Appl. Opt.* 37(26), 6196-6212 (1998).
3. O. Solgaard, F. S. A. Sandejas, and D.M. Bloom, "Deformable Grating Optical Modulator", *Opt. Lett.* 17(9), 688-690 (1992).
4. R. Fuchs, H. Jerominek, N. Swart, Y. Diawara, M. Lehoux, G. Bilodeau, S. Savard, F. Cayer, Y. Rouleau, P. Lemire, "Novel Beam Steering Micromirror Device", *Proc. SPIE* 3513, 40-49 (1998).
5. J.-H. Kim, L. Sun, C.-H. Jang, C.-C. Choi, R. T. Chen, "Polymer-Based Thermo-Optic Waveguide Beam Deflector with Novel Dual Folded-Thin-Strip Heating Electrodes," *Opt. Eng.* 42(3), 620-624 (2003).
6. D. Kang, J. E. MacLennan, N. A. Clark, A. Zakhidov and R. H. Baughman, "Electro-Optic Behavior of Liquid-Crystal-Filled Silica Opal Photonic Crystals: Effect of Liquid-Crystal Alignment", *Phys. Rev. Lett.* 86(18), 4052-4055 (2001).

7. P. Mach, P. Wiltzius, M. Megens, D. A. Weitz, K.-H. Lin, T.C. Lubensky, and A.G. Yodh, "Switchable Bragg Diffraction from Liquid Crystal in Colloid-Templated Structures", *Europhys. Lett.* 58(5), 679-685 (2002).
8. Miniewicz A., Gniewek A., and Parka J., "Liquid Crystals for Photonic Applications", *Optical Materials* 21(1-3), 605-610 (2002).
9. W. Klaus, "Development of LC Optics for Free-Space Laser Communications", *AEU-International Journal of Electronics and Communications* 56(4), 243-253 (2002).
10. S.-T. Wu, M. E. Neubert, S. S. Keast, D. G. Abdallah, S. N. Lee, M. E. Walsh, T. A. Dorschner, "Wide Nematic Range Alkenyl Diphenyldiacetylene Liquid Crystals", *Appl. Phys. Lett.* 77(7), 957-959 (2000).
11. A. B. Golovin, S.V. Shiyanovskii, and O.D. Lavrentovich, "Fast-Switching Dual-Frequency Liquid Crystal Optical Retarder, Driven by an Amplitude and Frequency Modulated Voltage", *Appl. Phys. Lett.* 83(19), p.3864-3866 (2003)
12. J. Borel, J. C. Deutsch, G. Labrunie, and J. Robert, "Liquid Crystal Diffraction Grating", US Patent 3,843,231 (22 October 1974).
13. G. Williams, N. J. Powell, A. Purvis, M. G. Clark, "Electrically Controlled Liquid Crystal Fresnel Lens", *Proc. SPIE* 1168, 352-357 (1989).
14. B. J. Cassarly, J. C. Ehlert, and D. J. Henry, "Low Insertion Loss High Precision Liquid Crystal Optical Phased Array", *Proc. SPIE* 1417, 110-121 (1991).
15. T. A. Dorschner and D. P. Resler, "Optical Beam Steering Having Subaperture Addressing", US Patent 5,093,740 (3 March 1992); T. A. Dorschner, "Method for Providing Beam Steering in a Subaperture-Addressed Optical Beam Steerer", US Patent 5,093,747 (3 March 1992).
16. E. Schulze and W. Reden, "Diffractive Liquid Crystal Spatial Light Modulators with Fine-Pitch Phase Gratings", *Proc. SPIE* 2408, 113-120 (1995).
17. W. Klaus, M. Ide, S. Morokawa, M. Tsuchiya, and T. Kamiya, "Angle-Independent Beam Steering Using a Liquid Crystal Grating with Multi-Resistive Electrodes", *Opt. Commun.* 138(1-3), 151-157 (1997).
18. X. Wang, D. Wilson, R. Muller, P. Maker, and D. Psaltis, "Liquid-Crystal Blazed-Grating Beam Deflector", *Appl. Opt.* 39(35), 6545-6555 (2000).
19. C. M. Titus, J. R. Kelly, E. C. Gartland, S. V. Shiyanovskii, J. A. Anderson, and P. J. Bos, "Asymmetric Transmissive Behavior of Liquid-Crystal Diffraction Gratings", *Opt. Lett.* 26(15), 1188-1190 (2001).
20. C. V. Brown, Em. E. Kriezis, and S. J. Elston, "Optical Diffraction from a Liquid Crystal Phase Grating", *J. Appl. Phys.* 91(6), 3495-3500 (2002).
21. J. J. Weinschenk, R. C. Hardie, S. R. Harris, "Restoration of Broadband Imagery Steered with a Liquid-Crystal Optical Phased Array", *Opt. Eng.* 41(10), 2613-2619 (2002).

22. E. Hallstig, L. Sjoqvist and M. Lindgren, "Intensity Variation Using a Quantized Spatial Light Modulator for Nonmechanical Beam Steering", *Opt. Eng.* 42(3), 613-619 (2003).
23. R. L. Sutherland, V. P. Tondiglia, L. V. Natarajan, T. J. Bunning, and W. W. Adams, "Electrically Switchable Volume Holographic Gratings in Polymer-Dispersed Liquid Crystals", *Appl. Phys. Lett.* 64(9), 1074-1076 (1994).
24. L. H. Domash, T. Chen, B. N. Gomatam, C. M. Gozewski, R. L. Sutherland, L. V. Natarajan, V. P. Tondiglia, T. J. Bunning, and W. W. Adams, "Switchable-Focus Lens in Holographic Polymer-Dispersed Liquid Crystals", *Proc. SPIE* 2689, 188-194 (1996).
25. P. Berthele, E. Gros, B. Fracasso, JLD De la Tochnaye, "Efficient Beam Steering in the 1.55 Micron Window Using Large-Tilt FLC One Dimensional Array", *Ferroelectrics* 214(1-2), 791-798 (1998).
26. M. Johansson, S. Hard, B. Robertson, I. Manolis, T. Wilkinson, W. Crossland, "Adaptive Beam Steering Implemented in a Ferroelectric Liquid-Crystal Spatial-Light-Modulator Free-Space, Fiber-Optic Switch", *Appl. Opt.* 41(23), 4904-4911 (2002)
27. D. Subacius, P. J. Bos, O. D. Lavrentovich, "Switchable Diffractive Cholesteric Gratings", *Appl. Phys. Lett.* 71(10), 1350-1352 (1997).
28. D. Subacius, S. V. Shiyonovskii, Ph. Bos, and O. D. Lavrentovich, "Cholesteric Gratings with Field-Controlled Period", *Appl. Phys. Lett.* 71(23), 3323-3325 (1997).
29. O. D. Lavrentovich, S. V. Shiyonovskii, and D. Voloschenko, "Fast Beam Steering Cholesteric Diffractive Devices", *Proc. SPIE* 3787, 149-155 (1999).
30. A. Y.-G. Fuh, C.-H. Lin, C.-Y. Huang, "Dynamic Pattern Formation and Beam Steering Characteristics of Cholesteric Gratings", *Jpn. J. Appl. Phys.* 41(1), 211-218 (2002).
31. Charles M. Titus, Philip J. Bos, Oleg D. Lavrentovich, "Efficient Accurate Liquid Crystal Digital Light Deflector", *Proc. SPIE* 3633, 244-253 (1999).
32. C.M. Titus, "Refractive and Diffractive Liquid Crystal Beam Steering Devices," *Dissertation, Chemical Physics Interdisciplinary Program, Kent State University*, pp. 34-36 (2000).
33. R. McRuer, L. R. Mcadams, J. W. Goodman, "Ferroelectric Liquid-Crystal Digital Scanner", *Opt. Lett.* 15(23), 1415-1417 (1990).
34. T. C. Lee and J. D. Zook, "Light Beam Deflection with Electrooptic Prisms", *IEEE Journal of Quantum Electronics* QE-4(7), 442-453 (1968).
35. H. Meyer, D. Riekman, K. P. Schmidt, U. J. Schmidt, M. Rahlff, E. Schroder, W. Thust, "Design and Performance of a 20-Stage Digital Light Beam Deflector", *Appl. Opt.* 11(8), 1732-1736 (1972).
36. R. Pepperl,"A Solid-State Digital Light Deflector with DKDP Polarization Switches", *Opt. Acta* 24(4), 413-25 (1977).

37. W. Kulchke, K. Kosanke, E. Max, M. A. Habberger, T. J. Harris, H. Fleisher, "Digital Light Deflectors", *Appl. Opt.* 5(10), 1657-67 (1966).
38. U. Kruger, R. Pepperl and U. J. Schmidt, "Electrooptic Materials for Digital Light Beam Deflectors", *Proceedings of the IEEE* 61(7), 992-1007 (1973).
39. L. M. Blinov, V. G. Chigrinov, *Electrooptic Effects in Liquid Crystal Materials*, Springer-Verlag New York, Inc. (1994).
40. P. G. de Gennes and J. Prost, *The Physics of Liquid Crystals*, 2nd ed., Clarendon Press, Oxford (1993).
41. G. Vertogen, W. H. de Jeu, *Thermotropic Liquid Crystals, Fundamentals*, Springer (1988).
42. M. Kleman and O. D. Lavrentovich, *Soft Matter Physics: An Introduction*, Springer NY, (2003).
43. G. R. Luckhurst, "Field-Induced Alignment of the Directors in the Smectic A Phase. Experiment and Simulation", *Mol. Cryst. Liq. Cryst.* 347(part II), 121-135 (2000).
44. G. R. Luckhurst, T. Miyamoto, A. Sugimura and B. A. Timimi, "Electric Field-Induced Alignment of the Directors in the Smectic A Phase of 4-Octyl-4'-Cyanobiphenyl. A Deuterium NMR Study", *Mol. Cryst. Liq. Cryst.* 347(part II), 147-156 (2000).
45. Y. Takanishi, Y. Ouichi, H. Takezoe, and A. Fukuda, "Chevron Layer Structure in Smectic A Phase of 8CB", *Jpn. J. Appl. Phys. Lett.* 28(3), L487-489 (1989).
46. O. D. Lavrentovich, M. Kleman and V. M. Pergamenschchik, "Nucleation of Focal Conic Domains in Smectic A Liquid Crystals", *J. Phys. II France* 4(2), 377-404 (1994).
47. O. D. Lavrentovich and M. Kleman, "Field-Driven First-Order Structural Transition in the Restricted Geometry of a Smectic A Cell", *Phys. Rev. E* 48(1), R39-R42 (1993).
48. Maurice Kleman and Oleg D. Lavrentovich, "Curvature Energy of a Focal Conic Domain with Arbitrary Eccentricity", *Phys. Rev. E* 61(2), 1574-1578 (2000).
49. Z. Li and O. D. Lavrentovich, "Surface Anchoring and Growth Pattern of the Field-Driven First-Order Transition in a Smectic-A Liquid Crystal", *Phys. Rev. Lett.* 73(2), 280-283 (1994).
50. O. Ou Ramdane, Ph. Auroy, S. Forget, E. Raspaud, Ph. Martinot-Lagarde, and I. Dozov, "Memory-Free Conic Anchoring of Liquid Crystals on a Solid Substrate", *Phys. Rev. Lett.* 84(17), 3871-3874 (1994).
51. F. A. Jenkins, H. E. White, *Fundamentals of Optics*, 4th ed., McGraw-Hill, Inc. (1976).
52. K. Hirabayashi, T. Yamamoto, M. Yamaguchi, "Free-Space Optical Interconnections with Liquid-Crystal Microprism Arrays", *Appl. Opt.* 34(14), 2571-2580 (1995).

53. C. H. Gooch and H. A. Tarry, "The Optical Properties of Twisted Nematic Liquid Crystal Structures with Twist Angles $\leq 90^0$ ", *J. Phys. D.: Appl. Phys.* 8(13), 1575-84 (1975); C. H. Gooch and H. A. Tarry, "Optical Characteristics of Twisted Nematic Liquid-Crystal Films", *Electron. Lett.* 10(1), 2-4 (1974).
54. A. B. Golovin, Y. Yin, S. V. Shiyanovskii, and O. D. Lavrentovich, "Fast Switching Dual Frequency Liquid Crystal Optical Retarder for Beam Steering Applications", *Proc. SPIE.* (to be published).
55. J.C. Bhatt, S.S. Keast, M.E. Neubert, R.G. Petshek, "Synthesis of Highly Chiral Multisubstituted Binaphthyl Compounds as Potential New Biaxial Nematic and NLO Materials", *Liq. Cryst.* 18(3), 367-380 (1995).

REPORT DOCUMENTATION PAGE			Form Approved OMB No. 0704-0188	
Public reporting burden for this collection of information is estimated to average 1 hour per response, including the time for reviewing instructions, searching existing data sources, gathering and maintaining the data needed, and completing and reviewing the collection of information. Send comments regarding this burden estimate or any other aspect of this collection of information, including suggestions for reducing this burden, to Washington Headquarters Services, Directorate for Information Operations and Reports, 1215 Jefferson Davis Highway, Suite 1204, Arlington, VA 22202-4302, and to the Office of Management and Budget, Paperwork Reduction Project (0704-0188), Washington, DC 20503.				
1. AGENCY USE ONLY (Leave blank)		2. REPORT DATE August 2004		3. REPORT TYPE AND DATES COVERED Technical Memorandum
4. TITLE AND SUBTITLE Digital Beam Steering Device Based on Decoupled Birefringent Prism Deflector and Polarization Rotator			5. FUNDING NUMBERS WBS-22-319-80-A5	
6. AUTHOR(S) Oleg Pishnyak, Lyubov Kreminska, Oleg D. Lavrentovich, John J. Pouch, Felix A. Miranda, and Bruce K. Winker				
7. PERFORMING ORGANIZATION NAME(S) AND ADDRESS(ES) National Aeronautics and Space Administration John H. Glenn Research Center at Lewis Field Cleveland, Ohio 44135-3191			8. PERFORMING ORGANIZATION REPORT NUMBER E-14696	
9. SPONSORING/MONITORING AGENCY NAME(S) AND ADDRESS(ES) National Aeronautics and Space Administration Washington, DC 20546-0001			10. SPONSORING/MONITORING AGENCY REPORT NUMBER NASA TM-2004-213197	
11. SUPPLEMENTARY NOTES Oleg Pishnyak, Lyubov Kreminska, and Oleg D. Lavrentovich, Liquid Crystal Institute, Kent State University, P.O. Box 5190, Kent, Ohio 44242-0001; John J. Pouch and Felix A. Miranda, NASA Glenn Research Center; and Bruce K. Winker, Rockwell Scientific Company LLC, 1049 Camino Dos Rios, Thousand Oaks, California 91360. Responsible person, John J. Pouch, organization code 5640, 216-433-3523.				
12a. DISTRIBUTION/AVAILABILITY STATEMENT Unclassified - Unlimited Subject Category: 74 Available electronically at http://gltrs.grc.nasa.gov This publication is available from the NASA Center for AeroSpace Information, 301-621-0390.			12b. DISTRIBUTION CODE	
13. ABSTRACT (Maximum 200 words) We describe digital beam deflectors (DBDs) based on liquid crystals. Each stage of the device comprises a polarization rotator and a birefringent prism deflector. The birefringent prism deflects the beam by an angle that depends on polarization of the incident beam. The prism can be made of the uniaxial smectic A (SmA) liquid crystal (LC) or a solid crystal such as yttrium orthovanadate (YVO ₄). SmA prisms have high birefringence and can be constructed in a variety of shapes, including single prisms and prismatic blazed gratings of different angles and profiles. We address the challenges of uniform alignment of SmA, such as elimination of focal conic domains. Rotation of linear polarization is achieved by an electrically switched twisted nematic (TN) cell. A DBD composed of N rotator-deflector pairs steers the beam into 2 ^N directions. As an example, we describe a four-stage DBD deflecting normally incident laser beam within the range of ±56 mrad with 8 mrad steps. Redirection of the beam is achieved by switching the TN cells.				
14. SUBJECT TERMS Liquid crystal; Beam steering; Polarization rotator; Beam deflector; Smectic A; Polarization rotator; Birefringent prism			15. NUMBER OF PAGES 28	
			16. PRICE CODE	
17. SECURITY CLASSIFICATION OF REPORT Unclassified	18. SECURITY CLASSIFICATION OF THIS PAGE Unclassified	19. SECURITY CLASSIFICATION OF ABSTRACT Unclassified	20. LIMITATION OF ABSTRACT	

